Exotic fluids and crystals of soft polymeric colloids



2002 J. Phys.: Condens. Matter 14 7681

(http://iopscience.iop.org/0953-8984/14/33/309)

INSTITUTE OF PHYSICS PUBLISHING JOURNAL OF PHYSICS: CONDENSED MATTER

J. Phys.: Condens. Matter **14** (2002) 7681–7698 PII: S0953-8984(02)38191-8

# Exotic fluids and crystals of soft polymeric colloids

**Christos N Likos**[1], **Norman Hoffmann**[1], **Hartmut Löwen**[1] **and Ard A Louis**[2]

[1] Institut für Theoretische Physik II, Heinrich-Heine-Universität Düsseldorf, Universitätsstraße 1, D-40225, Düsseldorf, Germany

[2] Department of Chemistry, University of Cambridge, Lensfield Road, Cambridge CB2 1EW, UK

Received 14 June 2002
Published 9 August 2002
Online at stacks.iop.org/JPhysCM/14/7681

**Abstract**

We discuss recent developments and present new findings in the colloidal description of soft polymeric macromolecular aggregates. For various macromolecular architectures, such as linear chains, star polymers, dendrimers, and polyelectrolyte stars, the effective interactions between suitably chosen coordinates are shown to be ultrasoft, i.e., they either remain finite or diverge very slowly at zero separation. As a consequence, the fluid phases have unusual characteristics, including anomalous pair correlations and mean-field-like thermodynamic behaviour. The solid phases can exhibit exotic, strongly anisotropic as well as open crystal structures. For example, the diamond and the A15 phase are shown to be stable at sufficiently high concentrations. Re-entrant melting and clustering transitions are additional features displayed by such systems, resulting in phase diagrams with a very rich topology. We emphasize that many of these effects are fundamentally different from the usual archetypal hard-sphere paradigm. Instead, we propose that these fluids fall into the class of mean-field fluids.

## 1. Introduction

One major advantage of soft-matter systems in comparison to their atomic counterparts is that one can engineer the constituent particles at the molecular level. In this way, an enormous variety of architectures can be achieved, leading to a corresponding richness in the structural and phase behaviour of such systems. Polymers play a prominent example within this class of materials. They come in a variety of forms, such as linear chain, branched, star-shaped, dendritic, and copolymer, as well as taking on a variety of functions, e.g., as steric stabilizers, additives, and depletants. Additional flexibility arises from it being possible to influence the structural and phase behaviour of polymer solutions by changing the solvent quality.

From the theoretical point of view, the task of bridging the gap between the microscopic and macroscopic length scales of polymeric systems is a formidable one. Indeed, the constituent

  

macromolecules may contain thousands or even millions of atoms, interconnected to one another in complicated ways. The programme of starting with the individual interactions between monomers and proceeding to the calculation of the free energy of the system rapidly becomes intractable. However, considerable progress can be made if one invokes a 'coarse-graining' procedure, an approach that has proved very fruitful in many areas of research in condensed matter physics. Here we follow a two-step procedure. First, instead of attempting to take a statistical trace over all the individual monomers in one step, one invokes a certain generalized coordinate of the macromolecule considered as an effective point particle. Examples include the centre of mass of the polymer or some suitably selected monomer, as we explain below. All monomers belonging to the macromolecules are then traced out for a given, fixed configuration of the effective coordinates, which defines an *effective interaction* between these coordinates [1, 2]. Once this is achieved, the second step consists of viewing the macroscopic system as a collection of point particles interacting by means of the effective interaction. Now all known tools from the theory of atomic and molecular fluids can be employed to derive structural and thermodynamic quantities for the system under consideration.

In recent years, the programme sketched out above has been carried out with success for various polymeric systems. It has been found that the effective interactions obtained belong to a new class of ultrasoft potentials which have very unusual properties when compared with the hard-sphere (HS) system, the prototype for atomic liquids. In this work, we first present a concise review of these novel properties for the fluid phases and then give some new results regarding the rich variety of crystal structures that can be stabilized by ultrasoft potentials. The rest of the paper is organized as follows. In section 2 we give the general definition of the effective interaction and present specific examples for a number of systems that have been worked out recently. In section 3 we show that the systems described by ultrasoft interactions are well described by a simple mean-field picture in the fluid phase for a wide range of thermodynamic conditions. To further delineate these systems we define two categories of mean-field fluids (MFF), the *strong* and the *weak* ones. The former are characterized by a direct correlation function $c(r)$ that satisfies to excellent accuracy the condition $c(r) = -\beta v(r)$ over broad regions of the thermodynamic space, where $v(r)$ is the interparticle pair potential. The latter conform to an approximate mean-field picture as regards only their thermodynamic properties, and not their structure. In section 4 we demonstrate that strong MFF can be further divided into two categories: those displaying re-entrant melting and those displaying a cascade of clustering transitions, the criterion being set by the positivity of the Fourier transform of the effective interaction. In section 5 we discuss the richness of the phase diagrams of weak MFF, taking the case of star polymers as a concrete example. Re-entrant melting as well as a wealth of structural phase transitions and exotic crystal phases are all shown to stem from the ultrasoftness of the effective interactions. Finally, in section 6 we summarize and conclude.

## 2. Effective interactions between polymeric macromolecules

The effective interaction between flexible, fluctuating aggregates can be given a precise statistical mechanical definition. Let us consider a solution containing $M$ polymeric macromolecules, each one of them composed of $N$ monomers. The total number of particles in the system is $\mathcal{M} = MN$. One starts from the full Hamiltonian $\mathcal{H}$ of the problem, assumed to be known. Then, out of the $\mathcal{M}$ particles in the problem (in our case all monomers), one selects the $M$ of them that are to be considered as 'effective particles' and holds them fixed in some prescribed configuration $\{\boldsymbol{R}_1, \boldsymbol{R}_2, \ldots, \boldsymbol{R}_M\}$, where $\boldsymbol{R}_i$ is the position of the $i$th effective particle. Afterwards, the $\mathcal{M} - M$ remaining particles are canonically traced out and the result

of this integration is a constrained partition function $Q(\boldsymbol{R}_1, \boldsymbol{R}_2, \ldots, \boldsymbol{R}_M)$. The effective Hamiltonian $\mathcal{H}_{\rm eff}$ is defined as

$$\exp(-\beta\mathcal{H}_{\rm eff}) = Q(\boldsymbol{R}_1, \boldsymbol{R}_2, \ldots, \boldsymbol{R}_M), \tag{1}$$

where $\beta = (k_{\rm B}T)^{-1}$, with the absolute temperature $T$ and Boltzmann's constant $k_{\rm B}$. It can be shown [2] that such an effective Hamiltonian has two useful properties: it preserves the overall thermodynamics of the system and it guarantees that the correlation functions of any order between any of the $M$ remaining particles remain invariant, regardless of whether the expectation values are calculated with the original Hamiltonian $\mathcal{H}$ or with the effective one $\mathcal{H}_{\rm eff}$. Though the procedure of tracing out the $\mathcal{M} - M$ degrees of freedom necessarily generates interactions of all orders between the $M$ particles [3, 4], in many cases it is sufficient to truncate these at the pair level, introducing thereby the *pair potential approximation*. The great advantage of employing this point of view is that, in comparison with the original problem, the numbers of particles, $\mathcal{M}$, has been reduced by a factor $N$. In addition, whereas in the original problem the pair interactions between the monomers are quite complicated, due to the need to take into account the connectivity and architecture of the molecule, in the effective description the pair potential is spherically symmetric, depending only on the magnitude of the separation vector between the two effective coordinates. A new picture of the polymers emerges thereby in which the latter can be seen as ultrasoft colloids having a dimension of the order of their radius of gyration $R_{\rm g}$. This sets at the same time the characteristic length scale of the effective interaction between them. When the polymers are neutral, $R_{\rm g}$ is the only length scale appearing in this colloidal description, whereas if they carry charge, additional scales set, e.g., by the concentration of the solution, the counterions and/or the salt ions also come into play. We examine some characteristic cases below.

*Polymer chains.* Two possible choices for the effective coordinates have been investigated thus far. One possibility is to consider the effective interaction $v_{\rm com}(r)$ between the *centres of mass* of the linear chains, when these are kept fixed at a distance $r$ from one another. This was first done in the pioneering work of Flory and Krigbaum [5], who found a Gaussian interaction between the centres of mass. Although the functional form of the Flory–Krigbaum potential is correct, the dependence of the prefactor on the degree of polymerization $N$ is not: whereas the Flory–Krigbaum mean-field approach predicts an $N^{1/5}$-dependence the prefactor turns out to be $N$-independent for sufficiently large $N$, as can be easily seen from examining the polymer second virial coefficient. Standard scaling arguments show that the radius of gyration $R_{\rm g}$ is the only relevant length scale for the dilute and semi-dilute regimes of polymers in a good solvent [6]. This immediately implies that the second virial coefficient should scale as $B_2 \sim R_{\rm g}^3$, which, in turn, implies that the effective interaction must have an amplitude that is independent of $R_{\rm g}$ [7], at least in the scaling limit.

A number of simulational [8–10] as well as theoretical approaches [11] involving two self-avoiding chains reached the conclusion that the aforementioned interaction has a Gaussian form. The lack of divergence of this effective interaction at zero separation should not be surprising. Indeed, the centres of mass of two polymer chains can coincide without any of the monomers violating the excluded-volume conditions. In addition, it can be seen that the effective 'particles' that one chooses for the coarse-grained description of the system do not need to be real particles of the physical system.

Recently, Louis *et al* [12–14] have independently carried out state-of-the-art simulations involving not just two but $N_{\rm c}$ chains and varying the number of chains to cover a very broad range of concentrations, ranging from dilute solutions up to nine times the overlap concentration. They confirmed that the effective potential has a Gaussian-like form which at

zero density can be well approximated by

$$v_{\rm com}(r) = \varepsilon \exp[-(r/\sigma)^2], \tag{2}$$

where $\varepsilon = 1.87\, k_{\rm B}T$ and $\sigma = 1.08\, R_{\rm g}$. For higher densities a superposition of three Gaussians provides a very accurate fit [15], but the basic shape does not deviate much from the low-density Gaussian form. The rather weak density dependence can be shown to arise from the density-independent many-body forces [16]. Moreover, the same authors have shown that employing this effective interaction leads to a very accurate description of the thermodynamics (equation of state) of polymer solutions for a wide range of concentrations, thus confirming the validity of the idea that polymer chains can be viewed as soft colloids [14].

An alternative is to consider the end-monomers or the central monomers of the chains as effective coordinates [7]. General scaling arguments establish that in this case the effective interaction diverges logarithmically with the monomer–monomer separation $r$ [17]. When the central monomers are chosen, linear chains are equivalent to star polymers with $f = 2$ arms. Motivated by this analogy, Jusufi *et al* [18] derived the effective interaction $v_{\rm cm}(r)$ by combining monomer-resolved, off-lattice simulations with theoretical arguments. The sought-for interaction features in this case a logarithmic divergence for small separations, in full agreement with the scaling arguments, and crosses over to a Gaussian decay for larger ones:

$$v_{\rm cm}(r) = \frac{5}{18} k_{\rm B}T f^{3/2} \begin{cases} -\ln\left(\dfrac{r}{\sigma_{\rm s}}\right) + \dfrac{1}{2\tau^2\sigma_{\rm s}^2} & \text{for } r \leqslant \sigma_{\rm s}; \\ \dfrac{1}{2\tau^2\sigma_{\rm s}^2} \exp\left[-\tau^2(r^2 - \sigma_{\rm s}^2)\right] & \text{for } r > \sigma_{\rm s}, \end{cases} \tag{3}$$

where $\sigma_{\rm s} \cong 0.66\, R_{\rm g}$ and $\tau(f)$ is a free parameter of the order of $1/R_{\rm g}$ and is obtained by fitting to computer simulation results. For $f = 2$ the value $\tau\sigma_{\rm s} = 1.03$ has been obtained [18], which, together with the potential in equation (3) above, yields for the second virial coefficient of polymer solutions the value $B_2/R_{\rm g}^3 = 5.59$, in agreement with the estimate $5.5 < B_2/R_{\rm g}^3 < 5.9$ from renormalization group and simulations [14].

*Dendrimers.* By employing a simple, mean-field theory based on the measured monomer density profiles of fourth-generation dendrimers, a Gaussian function of the form (2) has been shown to accurately describe the effective interaction between the centres of mass of these dendrimers [19, 20]. The prefactor $\varepsilon$ has in this case a higher value than for linear polymers, $\varepsilon \cong 10\, k_{\rm B}T$. Small-angle neutron scattering (SANS) profiles from concentrated dendrimer solutions are reproduced very well theoretically, at least below the overlap concentration $c_*$.

*Star polymers.* By chemically anchoring $f$ linear chains on a common core, star polymers with functionality $f$ are constructed. In the theoretical analysis of the conformations and the effective interactions of stars, the finite size of the core particle is ignored, an excellent approximation when the chains are long. The natural choice for the effective coordinates is now the position of the central particle, i.e., of the star centre. For small functionalities, $f \lesssim 10$, Jusufi *et al* [18] have shown that the logarithmic–Gauss potential of equation (3) accurately describes the effective interaction. The decay parameter $\tau$ of the Gaussian is $f$-dependent; for details see [18]. For larger functionalities, $f \gtrsim 10$, the Daoud and Cotton [21] blob picture of the stars is valid and the star–star interaction potential $v_{\rm ss}(r)$ reads as [22, 23]:

$$v_{\rm ss}(r) = \frac{5}{18} k_{\rm B}T f^{3/2} \begin{cases} -\ln\left(\dfrac{r}{\sigma_{\rm s}}\right) + \dfrac{1}{1+\sqrt{f}/2} & \text{for } r \leqslant \sigma_{\rm s}; \\ \dfrac{\sigma_{\rm s}/r}{1+\sqrt{f}/2} \exp\left[-\dfrac{\sqrt{f}}{2\sigma_{\rm s}}(r - \sigma_{\rm s})\right] & \text{for } r > \sigma_{\rm s}, \end{cases} \tag{4}$$

with the 'corona diameter' $\sigma_s \cong 0.66\, R_g$. Both star–star potentials, the one valid for $f \lesssim 10$, equation (3), and the one valid for $f \gtrsim 10$, equation (4), show an ultrasoft logarithmic divergence as $r \to 0$. The strength of the divergence is controlled by the functionality $f$, so at the formal limit $f \to \infty$ the interaction (4) tends to the HS potential.

*Polyelectrolyte stars.* If the polymer chains of a star polymer contain ionizable groups, the latter dissociate upon solution in a polar (aqueous) solvent, leaving behind charged monomers and resulting in a solution consisting of charged star polymers and counterions. The resulting macromolecules are called polyelectrolyte (PE) stars. In PE stars the chains are stretched due to the Coulomb repulsion of the charged monomers. The degree of stretching and condensation of counterions on the rods depends on the amount of charge and on the Bjerrum length. For moderate to high charging fractions, the effective interactions between the centres of the PE stars have been analysed recently by means of computer simulations and theory [24, 25]. This interaction, $v_{pes}(r)$, is dominated by the entropic contribution of the counterions that remain trapped within the star corona. For a broad range of functionalities and charge fractions, it can be accurately described by the fit

$$\frac{v_{pes}(r)}{k_B T} = \frac{\tilde{C} f N_c}{1-\zeta} \begin{cases} \left[1 - \left(\frac{r}{\sigma}\right)^{1-\zeta}\right] + \frac{2}{5}\left[\left(\frac{r}{\sigma}\right)^{2-\zeta} - 1\right] + \frac{3(1-\zeta)}{5(1+\kappa\sigma)} & \text{for } r \leqslant \sigma; \\ \frac{3(1-\zeta)}{5(1+\kappa\sigma)}\left(\frac{\sigma}{r}\right)\exp[-\kappa(r-\sigma)] & \text{for } r \geqslant \sigma, \end{cases} \tag{5}$$

where $N_c$ is the number of counterions, $\sigma$ the corona diameter of the PE star, and $\kappa$ the inverse Debye screening length due to the free counterions. Finally, $\tilde{C}$ and $\zeta$ are fit parameters, where $0 < \zeta < 1$. The last condition ensures that the potential of equation (5) above tends to a finite value as $r \to 0$. Hence, once more we are dealing with an ultrasoft interaction that varies slowly as the particle centres approach one another.

Ultrasoft interactions therefore describe quite a number of different systems. Their common characteristic is that the constituent particles are polymers of various architectures that dominate the spatial extent of the aggregates. In other words, one expects similar ultrasoft interactions to appear also when one deals with core–shell particles, consisting of a solid core and a polymeric shell, whenever the thickness of the latter greatly exceeds the radius of the former. In addition, the ultrasoft interactions can be tuned by controlling the number of arms, the charge, the length of the chains, the generation number (in the case of dendrimers), etc. Hence, it is useful to explore the general characteristics of this family of potentials and the ramifications for the structural and thermodynamic properties of the fluid and crystal phases of such systems.

## 3. Mean-field fluids

Motivated by the fact that effective interactions between polymeric colloids can be *bounded* (i.e., finite at all separations $r$), we examine here in general the properties of systems characterized by pair potentials of the form

$$v(r) = \varepsilon\phi(r/\sigma), \tag{6}$$

with $\phi(x) < \infty$ for all $x$. In equation (6) above, $\varepsilon$ is an energy scale and $\sigma$ a length scale. Moreover, $v(r)$ is non-attractive, i.e., $\mathrm{d}\phi(x)/\mathrm{d}x \leqslant 0$ everywhere. We introduce dimensionless measures of temperature and density as follows:

$$t = \frac{k_B T}{\varepsilon} = (\beta\varepsilon)^{-1}; \tag{7}$$

$$\eta = \frac{\pi}{6}\rho\sigma^3 = \frac{\pi}{6}\bar{\rho}, \tag{8}$$

where $k_B$ is Boltzmann's constant and $\rho = N/V$ is the density of a system of $N$ particles in the volume $V$. We will refer to $\eta$ as the 'packing fraction' of the system.

The key idea for examining the high-temperature and/or high-density limit of such model systems in three and higher dimensions is the following. We consider in general a spatially modulated density profile $\rho(\boldsymbol{r})$ which does not vary too rapidly on the scale $\sigma$ set by the interaction. At high densities, $\rho\sigma^3 \gg 1$, the average interparticle distance $a \equiv \rho^{-1/3}$ becomes vanishingly small, and $a \ll \sigma$ holds, i.e., the potential is of extremely long range. Every particle is simultaneously interacting with an enormous number of neighbouring molecules and, in the absence of short-range excluded-volume interactions, the excess free energy of the system [26] can be cast in the mean-field approximation (MFA) as equal to the internal energy of the system [27]:

$$F_{\mathrm{ex}}[\rho] \cong \tfrac{1}{2} \int\int \mathrm{d}^3 r\, \mathrm{d}^3 r'\, v(|\boldsymbol{r} - \boldsymbol{r}'|)\rho(\boldsymbol{r})\rho(\boldsymbol{r}'). \tag{9}$$

The pair interaction $v(|\boldsymbol{r} - \boldsymbol{r}'|)$ is of entropic origin; formally, however, it is equivalent to the energy cost of keeping the particles separated at a distance $|\boldsymbol{r} - \boldsymbol{r}'|$; thus we call the double integral in equation (9) the internal energy, in analogy with the theory of simple liquids. The approximation becomes more accurate with increasing density. Then, equation (9) immediately implies that in this limit the direct correlation function $c(r)$ of the system, defined as [26]

$$c(|\boldsymbol{r} - \boldsymbol{r}'|; \rho) = -\lim_{\rho(r)\to\rho} \frac{\delta^2 \beta F_{\mathrm{ex}}[\rho(\boldsymbol{r})]}{\delta\rho(\boldsymbol{r})\,\delta\rho(\boldsymbol{r}')}, \tag{10}$$

becomes independent of the density and is simply proportional to the interaction; i.e.,

$$c(r) = -\beta v(r). \tag{11}$$

Using the last equation, together with the Ornstein–Zernike relation [28], we readily obtain an analytic expression for the structure factor $S(k)$ of the system:

$$S(k) = \frac{1}{1 + \bar{\rho} t^{-1} \tilde{\phi}(k\sigma)}, \tag{12}$$

where $\tilde{\phi}(q) = \int \mathrm{d}^3 x \exp(-\mathrm{i}\boldsymbol{q}\cdot\boldsymbol{x})\phi(x)$ is the Fourier transform of $\phi(x)$.

Bounded and positive-definite interactions were studied in the late 1970s by Grewe and Klein [29, 30]. The authors considered a Kac potential of the form

$$v(r) = \gamma^d \psi(\gamma r), \tag{13}$$

where $d$ is the dimension of the space and $\gamma \geqslant 0$ is a parameter controlling the range *and* strength of the potential. Moreover, $\psi(x)$ is a non-negative, bounded, and integrable function. Grewe and Klein showed rigorously that at the limit $\gamma \to 0$, the direct correlation function of a system interacting by means of the potential (13) is given by equation (11) above. The connection with the case that we are discussing here is straightforward: as there are no hard cores in the system or lattice constants to impose a length scale, the only relevant length is set by the density, equal to $\rho^{-1/3}$ in our model, and by the parameter $\gamma^{-1}$ in model (13). In this respect, the limit $\gamma \to 0$ in the Kac model of Grewe and Klein is equivalent to the limit $\rho \to \infty$ considered here.

Although the limit of Grewe and Klein corresponds to $t \to \infty$ and $\bar{\rho} \to \infty$, the relation (11) has been shown to be an excellent approximation at arbitrarily low temperatures for high enough densities [27] and for temperatures $t \gtrsim 1$ at practically *all densities* [31]. Hence, the MFA is valid over a vast range of the thermodynamic space of such systems, which

has led to their characterization as MFF [32]. Associated with the structural relation (11) are scaling relations of thermodynamic quantities, arising from the compressibility sum rule [28]:

$$f''(\rho) = -\tilde{c}(k=0;\rho) = -4\pi \int_0^\infty r^2 c(r;\rho)\,\mathrm{d}r, \tag{14}$$

where $f(\rho) = \beta F_{\mathrm{ex}}(\rho)/V$, and the primes denote the second derivative. From equations (11) and (14) it then follows that

$$f(\rho) = \frac{\beta\tilde{v}(0)}{2}\rho^2, \tag{15}$$

with $\tilde{v}(0) = 4\pi \int_0^\infty r^2 v(r)\,\mathrm{d}r$. This simple scaling is not at all equivalent to a second virial theory. In fact, simple virial expansions have a rather small radius of convergence for mean-field fluids [13, 32]. It then follows that the excess pressure, chemical potential, and compressibility satisfy the scaling relations $P_{\mathrm{ex}} \sim \rho^2$, $\mu_{\mathrm{ex}} \sim \rho$, and $\chi_{\mathrm{ex}} \sim \rho^{-2}$ [13, 27][3]. All of these relations stem from the validity of the strong *structural* MFA relation (11) which guarantees the validity of the weaker *thermodynamical* MFA relation (15). In what follows, we will argue that many ultrasoft systems can still satisfy the thermodynamic relation (15) approximately, *without* satisfying equation (11). To distinguish between the two classes, we now qualify the term 'MFF' and call the systems for which both the structural and thermodynamic MFA work well *strong MFF*. For such systems, for which the potentials are typically also bounded, the density functional of equation (9) has been extended to mixtures [13] allowing a straightforward and transparent analysis of the phase separation in the bulk, interfacial [33], and wetting properties [34] of such mixtures.

Let us now then turn our attention to interaction potentials such as those given in equations (3) and (4). These diverge at the origin slowly enough that the three-dimensional integral

$$\int \mathrm{d}^3 r\, v(r) = 4\pi \int_0^\infty r^2 v(r)\,\mathrm{d}r = \tilde{v}(0), \tag{16}$$

is finite and equal (by definition) to the value of the Fourier transform of the potential $\tilde{v}(k)$ at $k = 0$. It is now impossible to satisfy the strong mean-field condition of equation (11) everywhere. Indeed, the direct correlation function $c(r)$ has to remain finite at $r = 0$, whereas the pair potential diverges. Hence, as shown in figure 1(a), there will always exist a region in the neighbourhood of the origin in which equation (11) is violated. At the same time, it can be seen in this figure that the extent of this region shrinks with increasing density; hence the fluid becomes more 'strong mean-field'-like as it gets denser. The smaller $\tilde{v}(0)$, the lower the density at which the MFA for $S(k)$, equation (12), becomes a reasonable approximation.

The discrepancies between $c(r)$ and $-\beta v(r)$ become much less important when we turn our attention to the thermodynamics. To obtain the excess Helmholtz free energy, one needs only the *integral* of $r^2 c(r)$; see equation (14). As demonstrated in figure 1(b), upon multiplication with the geometrical factor $r^2$, the deviations of $c(r)$ from $-\beta v(r)$ become suppressed, so we can write, to a very good approximation,

$$\int_0^\infty \mathrm{d}r\, r^2 c(r;\rho) \cong -\int_0^\infty \mathrm{d}r\, r^2 \beta v(r). \tag{17}$$

Equation (17), together with (14), yields an approximate scaling of the excess free energy of the weak MFF with density that is identical to that of the strong MFF, equation (15). The

[3] Note that for polymers in a good solvent, $P_{\mathrm{ex}} \sim \rho^{3\nu/(3\nu-1)} \approx \rho^{2.3}$ in the semi-dilute regime. The density dependence of the pair potentials is necessary for properly describing this correction to simple MFF behaviour [14]. But this in turn implies that the extra factor 0.3 in the scaling of the pressure arises from the many-body interactions, since these are what cause the density dependence in the first place [16, 35].

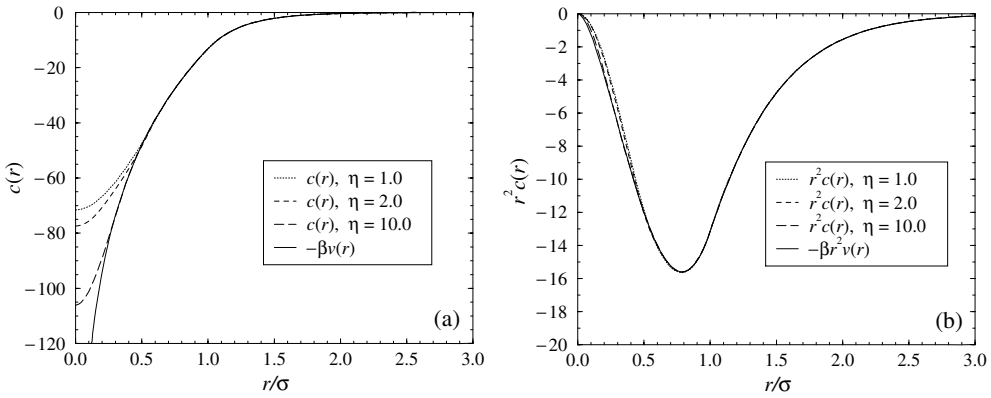


**Figure 1.** (a) Comparison between the direct correlation function of a $f = 32$ star polymer fluid at various densities, obtained by solving the Rogers–Young closure, with the mean-field result, $-\beta v(r)$. (b) As (a), but for the quantities $r^2c(r)$ and $-\beta r^2 v(r)$.

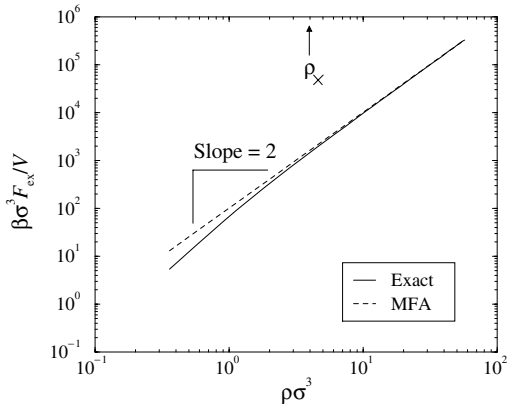


**Figure 2.** Comparison of the MFA (dashed line) with the exact result (solid line) for the excess free energy density of the $f = 32$ star fluid. The slope of the straight line is 2, indicating the quadratic dependence of the excess free energy density on the particle density. The arrow indicates the location of the crossover density $\rho_\times$, above which the scaling of equation (15) holds with a relative error of $<10\%$.

accuracy of the approximation for the star polymer fluid with $f = 32$ arms (equation (4)) is shown in figure 2. The line labelled as the exact free energy there was obtained by solving the Rogers–Young closure [36] for the fluid over a wide density range and subsequently utilizing the compressibility sum rule (equation (14)) to obtain the excess free energy. Comparisons with simulations [37] have indeed demonstrated that this procedure delivers an essentially exact numerical result. Here 'exact' refers to results within the confines of the pair potential approximation of equation (4).

Clearly, the MFA improves with increasing density, as the number of particles effectively interacting with one another grows. The crossover density $\rho_\times$ above which the quadratic scaling of the free energy holds is $f$-dependent and grows with increasing $f$. Indeed, the functionality acts as a prefactor that controls the strength of the logarithmic divergence of the potential at the origin. Formally, the MFA also becomes better with growing spatial dimension $d$, as the geometrical prefactor $r^{d-1}$ multiplying $c(r)$ and $-\beta v(r)$ suppresses the small-$r$

discrepancies of the two more efficiently. We call systems for which the mean-field idea holds only for the thermodynamics *weak MFF*. If one naively applies the *strong* mean-field relation, equation (11), to *weak* MFF, one obtains results for the structure factor $S(k) = [1 - \rho\tilde{c}(k)]^{-1}$ that can be seriously in error for finite $k$-values. *Only* at $k = 0$ and at sufficiently high densities is it a reasonable approximation to set $S(0) = [1 + \rho\beta\tilde{v}(0)]^{-1}$.

## 4. Clustering and re-entrant melting

In this section, we turn our attention to the phase behaviour of strong MFF. Two representatives of this class whose phase behaviour has been studied in detail are the Gaussian core model (GCM) of equation (2) and the 'penetrable sphere model' (PSM) characterized by the interaction potential $v_{\rm psm}(r) = \varepsilon\Theta(\sigma - r)$, with the Heaviside step function $\Theta(x)$. Clearly, the PSM reduces to the hard-sphere model for $t = 0$.

The GCM has been the subject of extensive investigations by Stillinger *et al* in the late 1970s [38–42]. The $t = 0$ phase diagram of the model was calculated, showing the existence of two stable crystal structures, fcc for low densities and bcc for high ones. In addition, a host of mathematical relations for the GCM have been established, and on the basis of free energy estimates is has been postulated that the system displays re-entrant melting behaviour at low temperatures. On the basis of simulation studies at selected thermodynamic points, a rough phase diagram of the GCM has been drawn [43]. A detailed study of the structural and phase behaviour of the GCM was carried out recently by Lang *et al* [27]. There, it was indeed shown that for temperatures $t > 0.01$ the system remains fluid at all densities, whereas for $t \leqslant 0.01$ re-entrant melting is observed: increasing the density, the system first undergoes a fluid $\rightarrow$ fcc transition, followed by a structural fcc $\rightarrow$ bcc transition and at higher densities the bcc solid remelts, i.e., a bcc $\rightarrow$ fluid transition takes place. The width of the solid-phase region grows with decreasing temperature. A structural signature of this unusual phase diagram in the fluid phase above $t = 0.01$ is an anomaly in the behaviour of the liquid structure factor $S(k)$. The height of its main peak first grows with increasing density and after achieving a maximum, it decreases again, reflecting the stability of the fluid beyond the re-entrant melting. The Hansen–Verlet freezing criterion [44, 45] was shown to be satisfied at *both* the freezing and the re-entrant melting lines [27]. Moreover, it was found that at high densities not only is the mean-field relation, equation (11), satisfied to excellent accuracy, but also the hypernetted chain closure (HNC) becomes quasi-exact [13, 27]. The system becomes 'quasi-ideal' at those densities, meaning that the radial distribution function has the limiting behaviour $g(r) \rightarrow 1$. This, in conjunction with the mean-field property $c(r) = -\beta v(r)$ and the exact relation $g(r) = \exp[-\beta v(r) - c(r) + g(r) - 1 + B(r)]$, forces the bridge function to obey the limit $B(r) \rightarrow 0$, hence rendering the HNC exact.

The PSM was first studied in detail by means of integral equation theories, computer simulations, and cell model calculations at small temperatures, $t \leqslant 0.3$ [46]. In contrast to the case for the GCM, no re-entrant melting was found. Instead, the freezing line of the system appeared to persist at all temperatures, and cascades of transitions in the solid were found, in which solids with multiple site occupancies are stable with increasing temperature and density, a phenomenon termed 'clustering' [31]. These findings were independently confirmed in a density-functional study of the low-temperature phase behaviour of the PSM [47]. Sophisticated integral equation approaches at arbitrarily high temperatures revealed a loss of the solution along the 'diagonal' $t = \eta$ of the phase diagram [48], again a feature pointing to an instability of the liquid with increasing density at arbitrarily high temperatures. Thus, the PSM and the GCM show completely different phase behaviours, although they are both bounded and non-attractive potentials. There is a cascade of clustering transitions for the

former, enabling freezing at all temperatures, and a re-entrant melting for the latter, associated with our inability to stabilize crystals above a certain maximum freezing temperature.

The key to understanding these two very different types of behaviour lies in the strong mean-field character of these fluids and the associated expression for the fluid structure factor, equation (12). If the Fourier transform of the pair interaction $\tilde{\phi}(k)$ has oscillatory behaviour (i.e., if $\tilde{\phi}(k)$ becomes negative for some $k$-values), then at the wavenumber $k_*\sigma$ where $\tilde{\phi}(k\sigma)$ attains its most negative value, $-|\tilde{\phi}(k_*\sigma)|$, the liquid structure factor $S(k_*)$ will display a maximum. For any given temperature $t$, there exists then a density $\bar{\rho}_s(t)$ such that $\bar{\rho}_s|\tilde{\phi}(k_*\sigma)| = t$, causing a divergence of the fluid structure factor at $k_*$ and marking a 'spinodal line' at this finite wavenumber. Thus, the fluid cannot be stable at all densities. In fact, freezing will take place before the spinodal line is reached. The PSM clearly belongs to this category, since the abrupt jump of the pair interaction $v_{\rm psm}(r)$ at $r = \sigma$ causes long-range oscillations of the potential in Fourier space. By employing the Hansen–Verlet criterion, $S(k_*) \cong 3$, it has been found [31] that in the PSM, freezing takes place at the 'diagonal' $t = \eta$ on which the integral equation approach of Fernaud *et al* [48] breaks down. If, on the other hand, the Fourier transform of the potential, $\tilde{\phi}(k)$ is a positive-definite, monotonically decreasing function of $k$, equation (12) ensures that at sufficiently high temperatures, where the MFA is valid at all densities [31], $S(k)$ is a monotonic function of $k$ approaching rapidly the value $S(k) = 1$ with increasing $k$ and devoid of any peaks. The lack of peaks in the structure factor implies the lack of any tendency within the liquid towards spontaneous formation of spatially modulated patterns. Thus, the fluid remains stable for all densities at sufficiently high temperatures. This, combined with the observation that at low temperatures and densities bounded potentials all become HS-like and hence they must cause a freezing transition there, leads to a re-entrant–melting scenario for such systems. Clearly, the GCM belongs to this category. Representative results for a particular family of strong MFF and schematic phase diagrams can be found in [31].

## 5. Exotic crystal phases

We now focus on weak mean-field fluids, for which no simple criterion for freezing behaviour can be established, since equations (11) and (12) are not satisfied any longer. The star polymer fluid characterized by the pair potential of equation (4) is a case in point[4]. The physical system of star polymers provides an excellent test-bed for the investigation of the thermodynamic stability of crystals more complicated than the usual fcc and bcc lattice arrangements.

The fcc lattice is the one favoured by hard interactions, since it has the property of maximizing the available volume and hence the entropy of the particles for a given particle density [49]. On the other hand, the presence of 'soft tails' in the potential has the effect of favouring the more open bcc lattice, as was convincingly demonstrated for the case of the screened Coulomb potential (Yukawa interaction) arising in charge-stabilized colloidal suspensions [50–53]. These two common lattices were considered for a long time to be the only 'candidates' in a search for stable crystals for given interatomic potentials. However, in modern colloidal science, new possibilities open up. It is technically possible to manufacture micelle-like particles featuring a hard core and a soft, fluffy corona of grafted or adsorbed polymer chains, with the thickness $L$ of the latter being much larger than the radius $R_c$ of the former. Star polymers correspond to the case $R_c \ll L$; the theoretical arguments leading to the

[4] We consider here the case $f > 10$, for which the interaction of equation (4) indeed holds, and not the low-functionality case for which the interaction of equation (3) is valid. The reason is that at low functionalities the stars do not freeze at any density and hence they are not an appropriate system for consideration when investigating thermodynamically stable crystals.

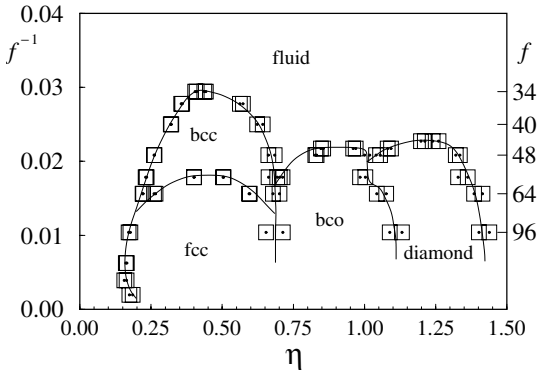


**Figure 3.** The phase diagram of star polymers. The symbols denote simulation results for the pairs of coexisting densities and the lines are guides to the eye. Notice that the density gaps at the phase boundaries are very narrow. (Redrawn from [54].)

effective potential of equation (4) are in fact based on the assumption $R_c \to 0$. Under these physical circumstances, the effective interaction between the micelles is dominated by the ultrasoft repulsion between the overlapping, flexible coronas and *not* by the excluded-volume interactions of the hard cores. Thereby, the requirement of maximizing of the volume available to each particle does not play the decisive role any longer.

These properties manifest themselves in the phase diagram of star polymer solutions. Due to the irrelevance of the temperature for these entropic interactions, the phase diagram was drawn in the $(f, \eta)$ plane by Watzlawek *et al* [54, 55], where $\eta = \pi\rho\sigma^3/6$ and $\rho = N/V$ is the number density of $N$ stars in the volume $V$. The phase diagram is shown in figure 3. The fluid phase remains stable at all concentrations for $f < f_{\min} = 34$, a result that confirms and makes precise early scaling-argument predictions of Witten *et al* [56]. For $f > f_c$ and at packing fractions $0.15 \lesssim \eta \lesssim 0.70$, the usual fcc and bcc crystals are seen to be stable, the former for larger and the latter for smaller functionalities. This is consistent with the fact that the effective potential of equation (4) has a Yukawa decay length scaling as $1/\sqrt{f}$; hence large $f$ is analogous to the strongly screened charge-stabilized colloidal suspensions. However, for $\eta \gtrsim 0.70$, unusual crystal structures appear. First, in the domain $0.70 \lesssim \eta \lesssim 1.10$, a body-centred orthogonal (bco) crystal is thermodynamically stable. The bco lattice is characterized by a body-centred, orthogonal conventional unit cell with three unequal sides and reduces to the bcc lattice for ratios 1:1:1 between the sides and to the fcc for ratios $1:1/\sqrt{2}:1/\sqrt{2}$ [57]. The bco lattices appearing in this region of the phase diagram feature strongly anisotropic unit cells with typical size ratios 1:0.6:0.3. Thus, these are crystals with coordination number 2. For packing fractions $1.10 \lesssim \eta \lesssim 1.50$, the diamond lattice with coordination number 4 turns out to be stable. Thus, we see that *very open* structures with their characteristically low coordination numbers are stabilized by the ultrasoft star–star potential. This feature has been attributed to the very slow divergence of the interaction as $r \to 0$, combined with its crossover to a Yukawa form for $r > \sigma$ [2, 54, 55]. Indeed, in such circumstances it may be energetically preferable for the system to have a small number of nearest neighbours at a small distance from any given lattice point rather than a large number of neighbours at a greater distance, as is the case for the optimally packed fcc lattice.

In the fluid there exist clear structural signatures both for the topology of the phase diagram of figure 3 and for the variety of the crystal phases featured there. The re-entrant transition from a fluid to a bcc lattice and then again to a fluid, occurring for $34 \lesssim f \lesssim 48$, is manifested

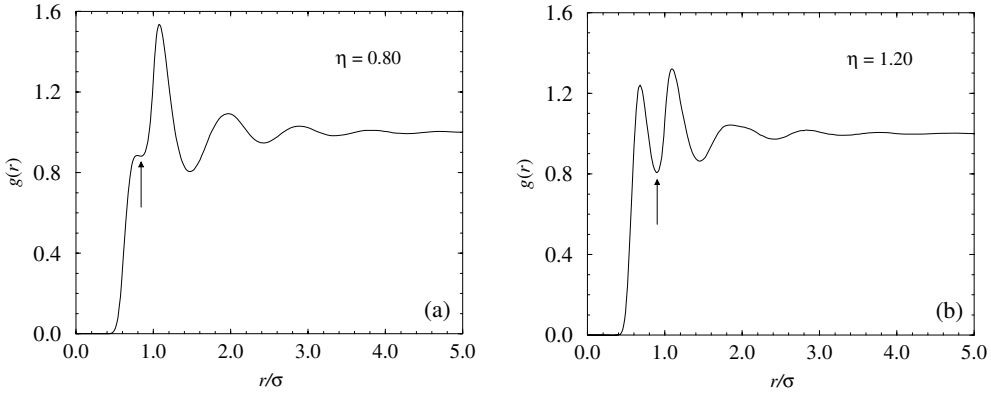


**Figure 4.** The radial distribution function of a star polymer fluid of functionality $f = 32$ at two different packing fractions, $\eta = 0.80$ (a) and $\eta = 1.20$ (b). The arrows indicate the positions $r_{\min}$ that define the borderline of the first coordination shell in the fluid phase.

in fluid structure factors $S(q)$ that show a main peak that first grows with increasing density and then drops again [37], as in the case of the GCM mentioned above. Moreover, once more the Hansen–Verlet freezing criterion [44, 45] was found to be satisfied on both sides of the freezing and re-entrant melting line. The radial distribution function $g(r)$ of the fluid at various densities, on the other hand, carries the signature of a local coordination that resembles that of the thermodynamically neighbouring solids. To demonstrate this, we show in figure 4 the function $g(r)$ for star polymer fluids at $f = 32$, which are thermodynamically stable, at packing fractions $\eta = 0.80$ and 1.20. Comparison with figure 3 shows that the former corresponds to a state at the vicinity of the bco phase and the latter to one in the vicinity of the diamond phase. Consider now the average coordination number $z$ in the fluid phase, defined as

$$z = 4\pi\rho \int_0^{r_{\min}} r^2 g(r)\,\mathrm{d}r, \tag{18}$$

where $r_{\min}$ is the position for which $g(r)$ has its first minimum and is indicated by the arrows in figure 4. For the two packing fractions shown, we obtain $z = 1.95$ at $\eta = 0.80$ and $z = 4.03$ at $\eta = 1.20$. The first is very close to the coordination number $z_{\mathrm{bco}} = 2$ of the neighbouring bco lattice and the latter to that, $z_{\mathrm{diam}} = 4$, of the diamond lattice. The fluid distribution functions contain local correlations that point to ordering of the incipient crystal phases.

The $g(r)$s of the fluid above the overlap density, $\eta \gtrsim 1.0$, show in addition anomalous behaviour featuring two distinct length scales, as is clear from figure 4(b). As analysed in detail in [37], two characteristics of the interaction are responsible for this behaviour: on the one hand, the existence of the crossover of the interaction of equation (4) at $r = \sigma$ from a logarithmic to an exponentially decaying form; and on the other, the ultrasoftness of the logarithmic potential, allowing the existence of fluids at arbitrarily large densities (for $f < f_{\min}$), a feature unknown for the usual interactions appearing in liquid-state physics and which are all 'perturbations' of the HS potential (e.g., Lennard-Jones, inverse powers). Thus, ultrasoft potentials carry unique structural signatures which should in principle be visible in scattering experiments on soft, polymeric fluids.

A great deal of insight into the general physical mechanisms driving the stability of open structures in soft systems was gained through the recent work of Ziherl and Kamien [58, 59]. They considered in full generality systems with particles composed of a hard core and long, deformable coronas and argued as follows. At any given density above the overlap

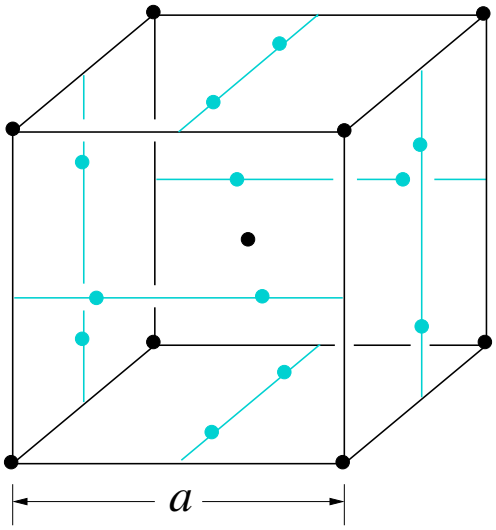


**Figure 5.** The conventional unit cell of the A15 lattice.

concentration, the coronas are forced to overlap and compress, which gives rise to an entropic free energy cost. This compressional penalty decreases with increasing thickness $d$ of the coronas. At the same time, the volume available to the coronal layer is fixed and given by the following difference: the total volume of the system minus the inaccessible volume of the hard cores. An estimate for this fixed available volume $V_{\text{free}}$ is given by the product of the total area $A$ of an imaginary membrane separating the compressed coronas multiplied by the average thickness $d$, $Ad = V_{\text{free}} = \text{constant}$. Since the cost for the compression of the chains grows with decreasing $d$, it turns out that favourable phases are those for which the interfacial area $A$ is minimal. Thereby, the problem reduces to that of determining the ordered arrangement of point particles that generates Wigner–Seitz (WS) cells having the smallest possible area for a given density. It is then conceivable that the fcc lattice will be disfavoured, since its WS cell has a larger area than that of the bcc one, for instance. In this way, Ziherl and Kamien established a beautiful connection of this problem with Lord Kelvin's celebrated question of determining the area-minimizing partition of space for an arrangement of soap bubbles of equal volume [60].

Following these arguments, it then turns out that there exists yet another candidate phase that has an area even smaller than the bcc lattice [61], namely the A15 lattice [62]. Self-assembled micelles of dendritic molecules with a particular architecture have been experimentally seen to crystallize into this phase [63]. The conventional unit cell of the A15 lattice is shown in figure 5. It can be thought of as the cell of a bcc lattice (dark points) decorated with 'dimers' (light points) running along the middle of the faces. The dimers are oriented parallel on opposite phases, forming thus columns through space. The orientations of the dimers lying on intersecting faces are perpendicular to one another, so one third of all dimers lie along each of the three Cartesian directions in space. The dimer length is $a/2$, where $a$ is the edge length of the cube, and it is placed symmetrically along the face, i.e., the distance of any monomer to its nearest edge is $a/4$. The A15 lattice is not a Bravais lattice; it can be constructed as a simple cubic (sc) arrangement with an eight-member basis; thus it

contains eight sites per conventional cell. Its WS cell is a Goldberg decatetrahedron[5] consisting of two hexagonal and twelve pentagonal faces [59].

Semi-quantitative calculations on the stability of the A15 lattice were carried out by Ziherl and Kamien [59], using a model 'square-shoulder' potential within a simplified cell model. Narrow regions in thermodynamic phase space were found, in which the A15 lattice was stable, but this finding is uncertain in view of the approximations involved and the limited extent of this region. To investigate this question in more detail, we have employed extensive lattice-sum calculations for the star polymer system, using the pair potential of equation (4) and extending both the set of candidate lattices and the region of densities that we looked at. We compared between the sc, diamond, bco (which includes the fcc and bcc lattices as special cases), and A15 lattices in the regions $0 \leqslant \eta \leqslant 2.50$ and $32 \leqslant f \leqslant 256$, at selected arm numbers $f$ to be shown below. The lattice sums were performed by fixing the particles at the prescribed lattice positions and keeping them frozen there, i.e., no thermal fluctuations (harmonic corrections) were taken into account. This approach reproduces very well the solid part of the phase diagram of figure 3: the free energy of the star polymer crystals turns out to be dominated by the lattice-sum term, the corrections to it from the particle oscillations as well as the entropic contribution from the same playing only a minor role. In this way, we are of course unable to compare the solid free energies with those of the fluid; therefore no prediction about melting can be made. However, for large enough $f$, the interaction is steep enough that the system will be definitely in a crystalline phase for which the lattice sums provide an accurate prediction of the most stable structure among the candidates.

For the bco phases we minimized the lattice sums with respect to the two size ratios $r_1 = b/a$ and $r_2 = c/a$ between the edge lengths, $a$, $b$, and $c$, at any given density. Without loss of generality, we assume in what follows that $a$ is the longest of the three edges; thus $0 < r_1, r_2 \leqslant 1$. The minimized bco energy was then compared with the energies of all other lattices; the one with the smallest lattice energy per particle wins.

The 'zero-temperature' phase diagram[6] obtained this way is shown in figure 6. First, we note that the phases that are stable up to $\eta \cong 1.50$ are precisely those also seen in the finite-temperature phase diagram of figure 3, and also that the phase boundaries based on the lattice sums agree very well with the ones at finite temperatures. The A15 phase does not alter the hitherto explored part of the phase diagram. However, for $\eta \gtrsim 1.50$, a host of new phases and of transitions between them appear. The A15 phase is stable in the high-density part of the phase diagram, thus confirming explicitly the prediction of [58] and [59] that this phase is a suitable candidate at high concentrations of ultrasoft particles. Nested between the stability domains of the A15 lattice and the diamond lattice, four new bco phases and (iso)structural transitions between them appear, having the following characteristics.

The phase denoted as $\mathrm{bco}_2$ has size ratios $r_1 = 1$ and $r_2 \cong 0.55$, the former being constant at all densities and functionalities and the latter showing very weak variation; see also figure 7. Hence, the unit cell of the $\mathrm{bco}_2$ phase is anisotropic only in one Cartesian direction, and has a wide base and a height that is less than the base edge length. Accordingly, the coordination number of this phase is 2. The $\mathrm{bco}_3$ phase, dominating at high functionalities, has size ratios

[5] We prefer the term *decatetrahedron* for a polyhedron with 14 faces to the term *tetrakaidecahedron*, often employed in the literature. The latter, inspired by ancient Greek, literally means 'four-and-ten-faced polyhedron', whereas the former, consistent with modern Greek, has the much more logical translation 'fourteen-faced polyhedron'. One of us (CNL) believes that the modern Greek language deserves a fair chance against its classical predecessor, which has influenced scientific terminology for quite some time.

[6] 'Zero-temperature' is just a convenient way to refer to the assumption of frozen particles at the lattice sites and does not refer to the *real* temperature $T$ of the system. The latter is an irrelevant thermodynamic variable because the entropic interaction of equation (4) is proportional to $k_\mathrm{B}T$ and the thermal energy is the *only* energy scale of the problem.

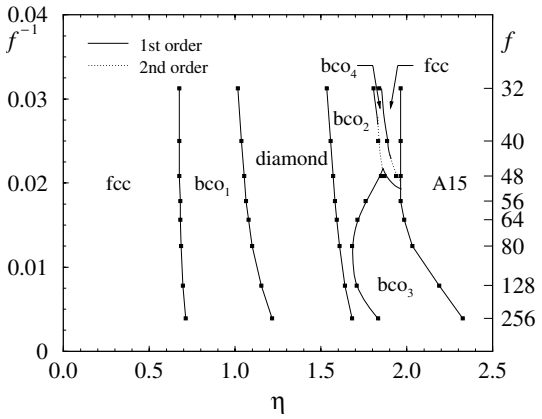


**Figure 6.** The zero-temperature phase diagram of star polymer solutions, obtained after the minimization of lattice sums for particles interacting by means of the potential of equation (4). The phase denoted as $\mathrm{bco}_1$ in this figure is the same as the one denoted as bco in figure 3 but now it has to be distinguished from the additional bco phases showing up at higher densities and named $\mathrm{bco}_2$, $\mathrm{bco}_3$, and $\mathrm{bco}_4$.

$r_1 = r_2 \cong 0.3$ which also show very little variation with $\eta$ and $f$; see figure 7. Similarly to that of the $\mathrm{bco}_2$ phase, therefore, the cell of the $\mathrm{bco}_3$ phase also has anisotropy in only one Cartesian direction. In contrast to the case for the $\mathrm{bco}_2$ phase, however, the height of the cell is now *larger* than the edge length of the base and therefore the number of nearest neighbours is 4. The phase transition $\mathrm{bco}_2 \rightarrow \mathrm{bco}_3$ is first order: as can be seen in figures 7(c) and (d), the size ratios jump abruptly from the values (1, 0.55) for $\mathrm{bco}_2$ to the values (0.3, 0.3) for $\mathrm{bco}_3$. These are the only stable bco phases in this part of the phase diagram as long as $f \gtrsim 56$.

For functionalities $32 \leqslant f \lesssim 56$, two more bco phases appear. First, there is a narrow region occupied by the $\mathrm{bco}_4$ phase, which has all three edge lengths of its unit cell different and is thus similar to the $\mathrm{bco}_1$ phase discovered before. As seen in figures 7(a)–(c), these ratios evolve from the values $r_1 = 1$ and $r_2 \cong 0.55$ of the $\mathrm{bco}_2$ phase towards the values $r_1 = 1/\sqrt{2}$ and $r_2 = 1/\sqrt{2}$ of the fcc phase.

The order of the transitions between those phases has been investigated numerically. Within the limits of accuracy of our numerical code, we have found that for $f = 32$ and 40 the transition $\mathrm{bco}_4 \rightarrow$ fcc is first order, i.e., the size ratios of the $\mathrm{bco}_4$ phase jump with increasing density to the ratios $r_1 = r_2 = 1/\sqrt{2}$ of the fcc phase abruptly. This is seen in figures 7(a) and (b). For $f = 48$, the transition is second order with the $\mathrm{bco}_4$ size ratios evolving to the fcc ones smoothly; see figure 7(c). The nature of the transition $\mathrm{bco}_2 \rightarrow \mathrm{bco}_4$ is also mixed. For $f = 32$ (figure 7(a)), a finite jump of the values of the ratios was found, although the step size in changing the packing fraction was made as small as $5 \times 10^{-5}$. Thus, we characterize this transition at $f = 32$ as first order. For $f = 40$ (figure 7(b)), this transition appears to be second order. Hence, we conclude that there must be a line of second-order transitions terminating at a tricritical point between $f = 40$ and 32 (for the $\mathrm{bco}_2 \rightarrow \mathrm{bco}_4$ transition), and similarly a tricritical point between $f = 48$ and 40 (for the $\mathrm{bco}_4 \rightarrow$ fcc transition), to be succeeded by lines of first-order transitions.

All four bco phases and the three transitions among them, $\mathrm{bco}_2 \rightarrow \mathrm{bco}_3 \rightarrow \mathrm{bco}_4 \rightarrow$ fcc, appear only in a very narrow $f$-range around $f = 48$; see figure 7(c). The line of second-order transitions $\mathrm{bco}_2 \rightarrow \mathrm{bco}_4$ meets the lines of first-order transitions $\mathrm{bco}_2 \rightarrow \mathrm{bco}_3$ and $\mathrm{bco}_3 \rightarrow \mathrm{bco}_4$ at a critical end-point located at $f$ slightly less than 48. Similarly, the line of second-order transitions $\mathrm{bco}_4 \rightarrow$ fcc also terminates at a critical end-point, meeting the first-order lines of

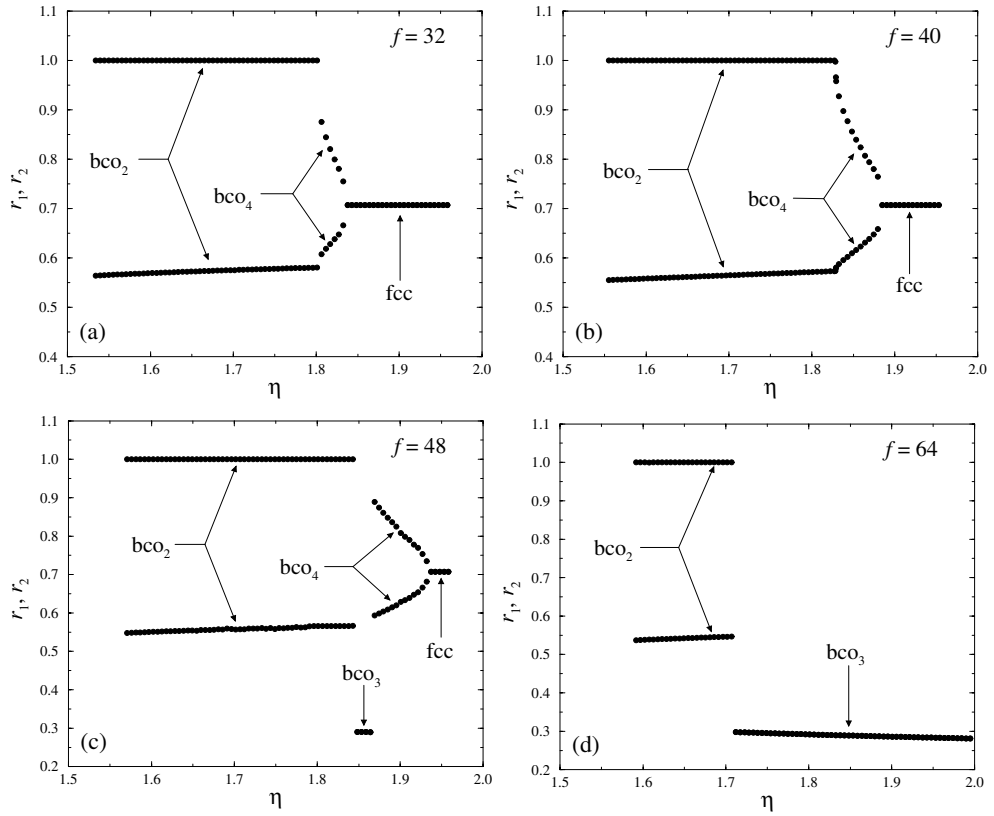


**Figure 7.** The optimal size ratios of the various bco phases occurring in the phase diagram of figure 6 between the diamond and the A15 phase, within their domains of stability. Also shown is the characterization of those phases. The four different functionalities are indicated on the plots.

$bco_3 \rightarrow$ A15 and fcc $\rightarrow$ A15. It is an intriguing phenomenon that such a richness in the stable crystal structures and in the nature of the transitions among them occurs as the result of a simple, spherically symmetric interaction, and this points to the many surprises of ultrasoft potentials and their tendency to produce open, exotic structures. At the same time, it must be pointed out that we do not expect the solid phases occurring for $f < 48$ to survive the competition with a fluid. Indeed, as can be seen from figure 3, the minimum freezing functionality $f_{\min}$ below which no solids are stable increases with increasing density. The bcc phase is extinguished by the fluid for $f < 34$, whereas the bco and diamond phases are extinguished for $f < 44$. It is therefore anticipated that the $bco_2$, $bco_4$, and fcc phases seen in figure 6 for $f < 48$ will be wiped out by the fluid there. However, by arbitrarily increasing $f$ one can always reach a domain where the fluid will be 'beaten' by the crystal and hence the $bco_2 \rightarrow bco_3 \rightarrow$ A15 transitions will be present also in the findings of a finite-temperature calculation. In particular, the A15 phase, whose stability has been speculated on for some time, has now been proved to indeed be the most stable phase at sufficiently high densities among the candidates considered.

The logarithmic–Yukawa potential employed in our study has been shown to describe well the effective interactions between star polymers in a good solvent for a wide range of concentrations. However, in the region of stability of the A15 crystal, the pair potential description is not expected to be particularly accurate. Many-body contributions are expected

to become important there [64]. Moreover, the Yukawa tail of the potential, describing the interactions of the outermost Daoud–Cotton blobs, should be absent, since the compressed coronas there are devoid of the outermost blob structure of the isolated stars. Thus, in this respect, the logarithmic–Yukawa potential has to be looked upon rather as a toy model. Nevertheless, the physical characteristic driving the transitions discovered above is the ultraslow divergence of the logarithm which, in the neighbourhood of the average particle distance can be locally expanded as a ramp-like potential, and the finer details of the interaction should become irrelevant.

## 6. Summary and conclusions

We have shown that 'ultrasoft interactions' arise naturally from coarse-graining procedures for a broad range of soft-matter systems. Besides greatly simplifying the statistical mechanics of these complex systems—once the interactions are derived, all the well known tools of liquid-state theory can be applied to calculate correlations and phase behaviour—they also lead to new phenomenology. Signatures of these ultrasoft interactions include anomalous fluid correlations, re-entrant melting, as well as the stabilization of exotic, open crystal structures. In contrast to their atomic counterparts, soft-matter systems can therefore stabilize such crystals without the presence of angle-dependent, anisotropic potentials: radially symmetric, ultrasoft interactions are quite sufficient. Thus, a new *mean-field fluid* paradigm can be established, which goes beyond the usual prototype for classical fluids, the HS model. The latter, being always dominated by packing effects, tends to favour close-packed structures. Exotic crystals with unusual ordering have been observed in HS-like suspensions [65, 66], but that case relates to *binary mixtures* whose phase behaviour is indeed much richer than that of their one-component counterparts.

## Acknowledgments

We thank Martin Watzlawek and Primoz Ziherl for helpful discussions. AAL thanks the Isaac Newton Trust, Cambridge, for financial support.

## References

[1] Pusey P N 1991 *Liquids, Freezing and Glass Transition (Les Houches Session LI)* ed J-P Hansen, D Levesque and J Zinn-Justin (Amsterdam: North-Holland)
[2] Likos C N 2001 *Phys. Rep.* **348** 267
[3] Dijkstra M, van Roij R and Evans R 1999 *Phys. Rev.* E **59** 5744
[4] Dijkstra M, Brader J M and Evans R 1999 *J. Phys.: Condens. Matter* **11** 10 079
[5] Flory P J and Krigbaum W R 1950 *J. Chem. Phys.* **18** 1086
[6] de Gennes P G 1979 *Scaling Concepts in Polymer Physics* (Ithaca, NY: Cornell University Press)
[7] Louis A A, Bolhuis P G, Finken R, Krakoviack V, Meijer E J and Hansen J-P 2002 *Physica* A **306** 251
[8] Grosberg A Y, Khalatur P G and Khokhlov A R 1982 *Makromol. Chem. Rapid Commun.* **3** 709
[9] Schäfer L and Baumgärtner A 1986 *J. Physique* **47** 1431
[10] Dautenhahn J and Hall C K 1994 *Macromolecules* **27** 5933
[11] Krüger B, Schäfer L and Baumgärtner A 1989 *J. Physique* **50** 3191
[12] Louis A A, Bolhuis P G, Hansen J-P and Meijer E J 2000 *Phys. Rev. Lett.* **85** 2522
[13] Louis A A, Bolhuis P G and Hansen J-P 2000 *Phys. Rev.* E **62** 7961
[14] Bolhuis P G, Louis A A, Hansen J-P and Meijer E J 2001 *J. Chem. Phys.* **114** 4296
[15] Bolhuis P G and Louis A A 2002 *Macromolecules* **35** 1860
[16] Bolhuis P G, Louis A A and Hansen J-P 2001 *Phys. Rev.* E **64** 021801
[17] Witten T A and Pincus P A 1986 *Macromolecules* **19** 2509

[18] Jusufi A, Dzubiella J, Likos C N, von Ferber C and Löwen H 2001 *J. Phys.: Condens. Matter* **13** 6177
[19] Likos C N, Schmidt M, Löwen H, Ballauff M, Pötschke D and Lindner P 2001 *Macromolecules* **34** 2914
[20] Likos C N, Rosenfeldt S, Dingenouts N, Ballauff M, Lindner P, Werner N and Vögtle F 2002 *J. Chem. Phys.* **117** 1869
[21] Daoud M and Cotton J P 1982 *J. Physique* **43** 531
[22] Likos C N, Löwen H, Watzlawek M, Abbas B, Jucknischke O, Allgaier J and Richter D 1998 *Phys. Rev. Lett.* **80** 4450
[23] Jusufi A, Watzlawek M and Löwen H 1999 *Macromolecules* **32** 4470
[24] Jusufi A, Likos C N and Löwen H 2002 *Phys. Rev. Lett.* **88** 018301
[25] Jusufi A, Likos C N and Löwen H 2002 *J. Chem. Phys.* **116** 11 011
[26] Evans R 1979 *Adv. Phys.* **28** 143
[27] Lang A, Likos C N, Watzlawek M and Löwen H 2000 *J. Phys.: Condens. Matter* **12** 5087
[28] Hansen J-P and McDonald I R 1986 *Theory of Simple Liquids* 2nd edn (London: Academic)
[29] Grewe N and Klein W 1977 *J. Math. Phys.* **64** 1729
[30] Grewe N and Klein W 1977 *J. Math. Phys.* **64** 1735
[31] Likos C N, Lang A, Watzlawek M and Löwen H 2001 *Phys. Rev.* E **63** 031206
[32] Louis A A 2001 *Phil. Trans. R. Soc.* A **359** 939
[33] Archer A J and Evans R 2001 *Phys. Rev.* E **64** 041501
[34] Archer A J and Evans R 2002 *J. Phys.: Condens. Matter* **14** 1131
[35] Louis A A 2002 *Preprint* cond-mat/0205110
[36] Rogers F A and Young D A 1984 *Phys. Rev.* A **30** 999
[37] Watzlawek M, Löwen H and Likos C N 1998 *J. Phys.: Condens. Matter* **10** 8189
[38] Stillinger F H 1976 *J. Chem. Phys.* **65** 3968
[39] Stillinger F H and Weber T A 1978 *J. Chem. Phys.* **68** 3837
[40] Stillinger F H 1979 *J. Chem. Phys.* **70** 4067
[41] Stillinger F H 1979 *Phys. Rev.* B **20** 299
[42] Stillinger F H and Weber T A 1978 *Phys. Rev.* B **22** 3790
[43] Stillinger F H and Stillinger D K 1997 *Physica* A **244** 358
[44] Hansen J-P and Verlet L 1969 *Phys. Rev.* **184** 151
[45] Hansen J-P and Schiff D 1973 *Mol. Phys.* **25** 1281
[46] Likos C N, Watzlawek M and Löwen H 1998 *Phys. Rev.* E **58** 3135
[47] Schmidt M 1999 *J. Phys.: Condens. Matter* **11** 10 163
[48] Fernaud M J, Lomba E and Lee L L 2000 *J. Chem. Phys.* **112** 810
[49] Hales T C 2000 *Not. Am. Math. Soc.* **47** 440
[50] Hone D, Alexander S, Chaikin P M and Pincus P 1983 *J. Chem. Phys.* **79** 1474
[51] Kremer K, Robbins M O and Grest G S 1986 *Phys. Rev. Lett.* **57** 2694
[52] Robbins M O, Kremer K and Grest G S 1988 *J. Chem. Phys.* **88** 3286
[53] Sirota E B, Ou-Yang H D, Sinha S K and Chaikin P M 1989 *Phys. Rev. Lett.* **62** 1524
[54] Watzlawek M, Likos C N and Löwen H 1999 *Phys. Rev. Lett.* **82** 5289
[55] Watzlawek M 2000 *Phase Behavior of Star Polymers* (Aachen: Shaker)
[56] Witten T A, Pincus P A and Cates M E 1986 *Europhys. Lett.* **2** 137
[57] Ashcroft N W and Mermin N D 1976 *Solid State Physics* (Philadelphia, PA: Holt-Saunders)
[58] Ziherl P and Kamien R D 2000 *Phys. Rev. Lett.* **85** 3528
[59] Ziherl P and Kamien R D 2001 *J. Phys. Chem.* B **105** 10 147
[60] Thomson W 1887 *Phil. Mag.* **24** 503
[61] Weaire D and Phelan R 1994 *Phil. Mag. Lett.* **69** 107
[62] Rivier N 1994 *Phil. Mag. Lett.* **69** 297
[63] Balagurusamy V S K, Ungar G, Percec V and Johansson G 1997 *J. Am. Chem. Soc.* **119** 1539
[64] von Ferber C, Jusufi A, Likos C N, Löwen H and Watzlawek M 2000 *Eur. Phys. J.* E **2** 311
[65] Bartlett P, Otewill R H and Pusey P N 1992 *Phys. Rev. Lett.* **68** 3801
[66] Bartlett P and Pusey P N 1993 *Physica* A **194** 415